Electron-temperature inhomogeneities along an x-ray laser plasma

B. La Fontaine,* J. Dunn,† H. A. Baldis,† G. D. Enright, and D. M. Villeneuve
Steacie Institute for Molecular Sciences, National Research Council of Canada, Ottawa, Canada K1A 0R6

J. C. Kieffer, M. Nantel, and H. Pépin
Institut National de la Recherche Scientifique (INRS-Énergie), P.B. 1020, Varennes, Quebec, Canada J3X 1S2
(Received 12 May 1992; revised manuscript received 19 August 1992)

The uniformity of electron temperature (T_e) along an x-ray laser plasma produced by a line-focused laser was investigated with precise space- and time-resolved measurements. Thomson scattering of a uv probe by the plasma was used to measure the spatial variation of T_e along the line focus. This characterization was complemented by spatially resolved L-shell x-ray spectroscopy. Electron temperatures obtained from the $n=4\rightarrow 2$ F-like to Ne-like line ratios agree well with the results from Thomson scattering. Interferometry and x-ray imaging were also used to aid in the diagnosis of the plasma. The inhomogeneities observed are typical of those to be expected in x-ray laser experiments and can lead to significant reduction of the inferred gain on the Ne-like transitions.

PACS number(s): 52.25.−b, 42.55.Vc, 52.70.−m, 32.30.Rj

I. INTRODUCTION

In the past eight years, the development of x-ray lasers has attracted world-wide attention. X-ray gain has been observed in a number of laboratories, for several atomic transitions [1–10]. In particular, much success has been obtained with collisionally pumped x-ray lasers. However, many aspects of these x-ray lasers are still not well understood [11]. The successful modeling of such systems comprises several steps: the determination of the plasma density, temperature and ionization balance, a knowledge of atomic physics rates pertinent to the inversion density, and the transport of the amplified extreme ultraviolet (XUV) light through the plasma. Experimental measurements of plasma parameters such as electron temperature and density of the gain region are therefore needed in order to provide accurate input to the models [12].

Studying the nonuniformities in x-ray laser plasmas is also very important. Indeed, degradation of the gain in the regions not adequately pumped is a serious problem for the optimization of these lasers [13,14]. Reducing inhomogeneities could relax the requirements on the pump laser and lead to a more compact x-ray laser system.

The results reported here form a quantitative study of the effect of illumination nonuniformity on the electron temperature (T_e) of a plasma in a line-focus geometry under conditions for which gain is observed. Preliminary measurements on line-focus copper plasmas have previously been reported [15]. The present study was realized independently from the gain measurements that were done on several $3p\rightarrow 3s$ transitions of a Ne-like Ge x-ray laser [9]. Even though the characterization of the plasma was performed in a separate experimental chamber, the conditions were similar to those where x-ray laser gain was measured [16]. The pattern of the beam used to create the plasma was not the same since a much shorter plasma was used here but the inhomogeneities are representative of those observed during the gain measurements.

Thermal Thomson scattering was used to measure the electron temperature in the plasma, with spatial and temporal resolution. At the same time, x-ray spectra of the keV region were recorded and served both as a temperature diagnostic and as a monitor of the charge state of the plasma. X-ray imaging was also used to aid in characterizing the inhomogeneities. Finally, uv interferometry provided an indication of the electron density.

II. EXPERIMENTAL ARRANGEMENT

The experiments were conducted at the National Research Council of Canada. For the experiments described in this paper, a Nd:glass laser system operating at a wavelength of 1.064 μm, with a Gaussian pulse of 2.5 ns full width at half maximum (FWHM), was used to create the x-ray laser plasma. This plasma was produced by focusing the laser beam onto a solid slab of germanium with a long-focal-length cylindrical lens and an $f/10$ aspheric lens. A line focus with focal spot dimensions of $(1.50\pm0.05$ mm$)\times(150\pm20$ μm) (FWHM) was thus produced. The laser energy varied between 60 and 80 J ($\pm10\%$), resulting in an average fluence on the target of $\sim 1.2\times10^{13}$ W/cm^2. Inhomogeneities of typically $\pm35\%$ on the intensity distribution at the focal spot were observed. The orientation of the line focus could be set as vertical or horizontal for the various shots, in order to accommodate the different diagnostics used. Throughout this paper the long axis of the plasma will be referred to as the x axis, regardless of its actual orientation, and the axis normal to the target surface will be identified as the z axis. The origin of the x axis is defined with respect to a fixed reference point at the edge of the target. For some shots, a spot-focus plasma with a diameter of 150 ± 20 μm

(FWHM) was used, with a laser energy of ~5 J. In this case, the cylindrical lens was removed from the laser beam path.

The experimental arrangement is shown in Fig. 1. The Thomson scattering diagnostic used a 2.5-ns FWHM probe with a wavelength of 355 nm and energy of ~0.5 J, synchronized with the main laser pulse. This uv beam, incident at an angle of 60° from the laser axis, was focused onto a 50-μm spot in the plasma, with an $f/5$ lens. The scattered light was collected at 90° from the probe with an achromatic $f/5$ uv lens which relayed the image of the plasma outside the interaction chamber. This image was then relayed again, with a spherical mirror, onto the entrance slit of a 1-m $f/10$ Czerny-Turner spectrometer. The spectral resolution, which was defined by the entrance slit of the spectrometer, was 0.5 Å. The resulting spectrum was then dispersed in time with a streak camera and recorded on film. The temporal resolution was 100 ps. The intersection of the 50-μm-diameter probe beam and a 70-μm-diameter area determined by the collecting optics defined the volume where the plasma parameters were probed. The electron temperature at different positions along the line focus was recorded by shifting the line focus along its long axis between shots.

X-ray spectroscopy in the keV range was performed simultaneously with a pentaerythritol PET(002), $2d = 8.74$ Å, flat crystal spectrometer located at 45° from the laser axis and at 55° below the horizontal plane. A slit placed in front of the crystal gave 50 μm spatial resolution along the line focus, perpendicular to the spectrometer axis of dispersion. The resolving power of $\lambda/\delta\lambda = 2000$ was determined by the lateral dimension of the line focus. The wave band of interest, 6.5–8.3 Å, included the $4d \rightarrow 2p$ Ne-like and F-like resonance lines. The spectra were recorded with Kodak DEF392 x-ray film filtered with a total of 37.5 μm of beryllium. The film calibration of Henke *et al.* [17], together with the measured crystal reflection integral data of Hall [18] and the filter transmission response [19], was included to give absolute x-ray emission in units of J Å^{-1} sr^{-1}. For line ratio comparisons, the total emission was integrated in each line.

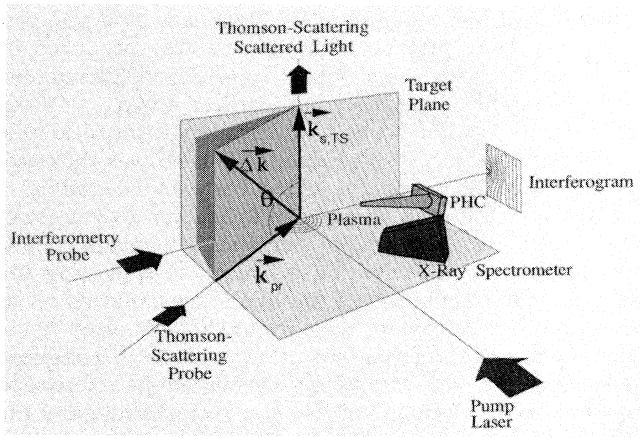

FIG. 1. Experimental setup. The diagnostics used were Thomson scattering of a uv probe by the plasma, x-ray spectroscopy, interferometry, and x-ray imaging. The vector diagram for Thomson scattering is shown. The line focus could be oriented either horizontally or vertically.

X-ray emission from the plasma was also monitored with a 7× magnification pinhole camera placed perpendicular to the main laser axis. The plasma images, with a spatial resolution of 20 μm, were filtered with 12.5 μm beryllium and recorded on Kodak RAR2495 film. Although the instrument was sensitive to emission from 1–15 Å, the images were weighted to the intense Ne-like and F-like $3d \rightarrow 2p$ resonance lines around 9 Å. The film calibration and development procedures of Henke *et al.* [20] were followed.

Interferometry complemented the plasma characterization. It was performed with a folded wave front interferometer and a 15-ps, 355-nm laser pulse probing parallel to the target surface, perpendicular to the x axis.

III. EXPERIMENTAL RESULTS

The effects of the illumination nonuniformity can be readily observed with the x-ray pinhole images of the plasma. A time-integrated image of the line-focus plasma is shown in Fig. 2. The peak emission, shown here, occurs at a position of $z = 50 \pm 10$ μm in front of the target plane as can be observed from a microdensitometer intensity profile (not shown) of the pinhole camera image along the z axis. The most intense emission along the line focus is measured at a position $x = 1.2$ mm corresponding to the maximum energy density distribution in the main laser beam (the "pump" laser). This also corresponds to the highest-temperature region as measured by the temperature diagnostic instruments (discussed below).

The electron temperature was measured with Thomson scattering [21,22]. For the conditions of this experiment, the scattering is predominantly from the thermal ion acoustic waves ($0.1 < \Delta k \lambda_{De} < 0.5$, where λ_{De} is the Debye length) [23]. The scattered light spectrum is characterized by two resonance peaks (the "ion feature") separated by twice the ion acoustic frequency $\omega_{IA} = \Delta k c_s$, where c_s is the ion sound speed which is a function of T_e. A sample streak record of a Thomson scattering spectrum, for which the volume probed was at the position $x = 2.20 \pm 0.15$ mm along the line focus and $z = 50 \pm 25$ μm away from the target surface, is presented in Fig. 3(a). One can clearly see in this figure the two peaks of the ion feature. The central line is caused by stray light at the probe frequency. The background light is due to the continuum emission of the plasma. Figure 3(b) shows an intensity profile of this streak record, at the peak of the laser pulse ($t = t_{peak} \pm 100$ ps).

By fitting a theoretical spectrum to the experimental one, one can obtain the electron temperature. The parameters required for the fit are T_e and T_i (the electron and ion temperatures), v_{di} and v_{de} (the ion and electron drift velocities), n_e (the electron density), and $\bar{Z}$ (the average ion charge). $\bar{Z}$ can be estimated from the x-ray spec-

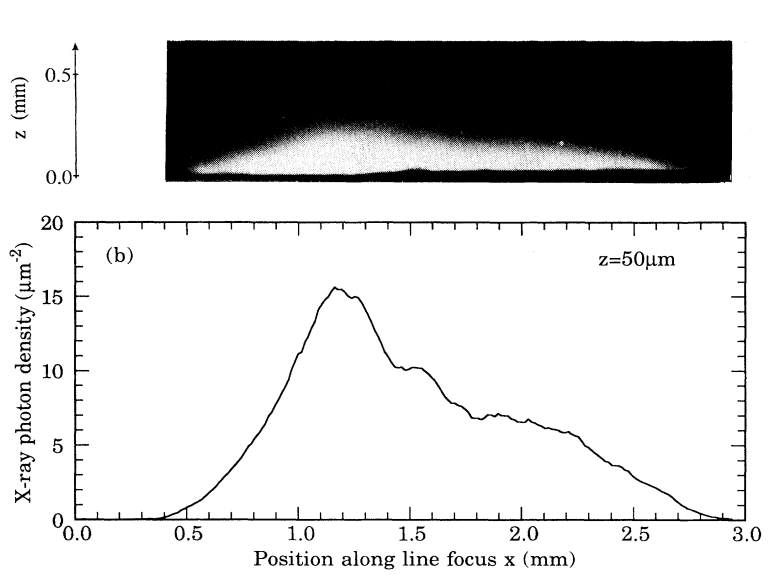

FIG. 2. This line rendition of the x-ray image of the line-focus plasma taken at $z=50\pm10$ μm from the target plane shows the inhomogeneities along the line focus. The x-ray photon density is expressed in photons/μm^2 at the film plane.

tra. For the plasmas probed during this experiment, $\bar{Z}=22\pm1$. The electron density is obtained through interferometric measurements done in spot-focus geometry and from hydrodynamic simulations. These estimates should be accurate to within a factor of 2 or 3. This uncertainty of n_e can result in an error of $<5\%$ on $\Delta k \simeq 2k_{\rm pr}\sin(\theta/2)$, where $k_{\rm pr}\cong\omega_{\rm pr}/c(1+n_e/9n_c)^{1/2}$ is the wave-vector amplitude of the probe ($n_c=1\times10^{21}$ cm^{-3} is the critical density for the pump laser). The range of Δk allowed by the f numbers of the probe beam focusing and collecting optics is also $\sim5\%$. We estimate that the possible error on the T_e inferences, due to the above-mentioned uncertainties, is less than 10%. The other parameters relevant to the calculation of the spectrum, T_i, v_{di}, and v_{de}, are weakly correlated to T_e. Therefore they have little effect on the deduced T_e value. Even though the ion temperature is one of the parameters needed for the evaluation of the theoretical spectrum, it was not possible to obtain a good estimate of T_i for this experiment. This is discussed in more length in the next section. More details of the fitting process may be found elsewhere [24,25].

The x-ray spectrometer could also provide an estimate of the electron temperature T_e and monitor the state of ionization of the line-focus plasma at different positions simultaneously. Three spectra are shown in Figs. 4(a), 4(b), and 4(c), each corresponding to a different line-focus position at $x=1.3$, 1.9, and 2.75 mm (±0.1 mm), respec-

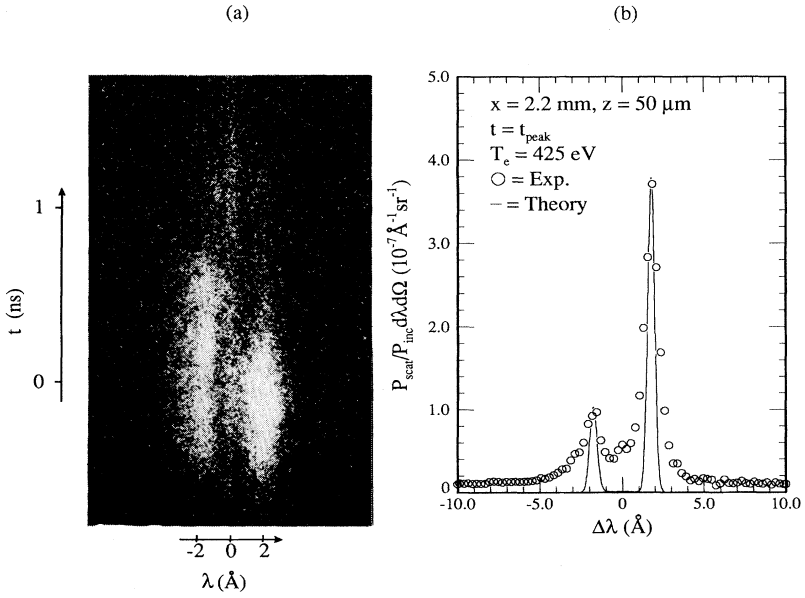

FIG. 3. Thomson scattering spectrum from Ne-like Ge x-ray laser plasma. $I=1\times10^{13}$ W/cm^2, $x=2.20\pm0.15$ mm, and $z=50\pm25$ μm. (a) Streak record showing the two peaks of the ion feature. (b) Intensity profile taken at $t=0\equiv t_{\rm peak}$. ($T_e=425\pm60$ eV.)

tively. An interesting observation is the significant variation in emission of the F-like $3p \rightarrow 2s$ and $4d \rightarrow 2p$ resonance lines with position. Previous spectroscopic studies of line-focus Cu plasmas have shown a similar behavior for F-like Cu emission [15]. Towards the edge of the line focus at $x = 2.75$ mm, Fig. 4(c), the F-like Ge emission is almost completely absent; the spectrum is dominated by the $n = 4 \rightarrow 2$ Ne-like transitions and associated Na-like satellites. At peak irradiance position [Fig. 4(a)], strong F-like and O-like emission is observed around the 8.0- and 6.8-Å regions. As will be shown later, the change in

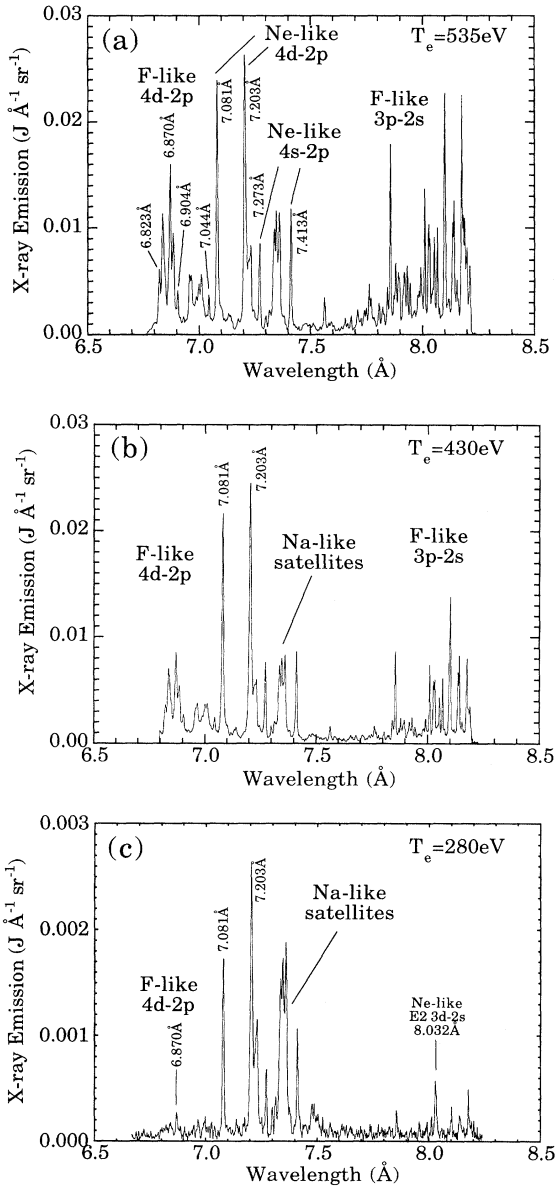

FIG. 4. X-ray spectra (a), (b), and (c) taken at three different line-focus positions $x = 1.3$, 1.9, and 2.75 mm, respectively. F-like $4d \rightarrow 2p$ transitions used in the temperature calculation, are labeled along with the Ne-like $4d \rightarrow 2p$ and $4s \rightarrow 2p$ transitions.

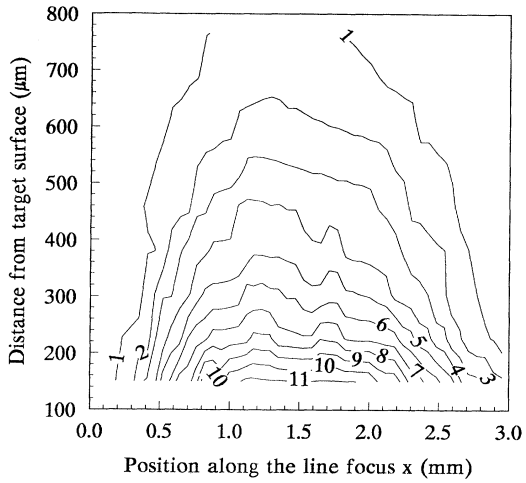

FIG. 5. Interferometric image of the plasma. Plotted here is the phase shift in multiples of wavelengths experienced by the probe beam as it passes through the plasma.

F-like ion emission with line-focus position is a result of electron-temperature inhomogeneities. This has further significance, since the observation of gain on $3p \rightarrow 3s$ lasing lines is strongly correlated with the presence of the F-like Ge lines [9,26] in the $n = 3 \rightarrow 2$ spectrum: the interpretation of this phenomenon is that the electron-temperature threshold for significant collisional pumping of the $n = 3$ levels, from the ground state, has been exceeded.

Finally, interferometry was used to qualitatively describe the behavior of the electron density in the presence of illumination nonuniformity. A phase-shift map, showing the phase shift experienced by the probe beam as it passes through the plasma, taken at $t = t_{peak} + 350$ ps (± 200 ps), is depicted in Fig. 5. One notices that the fringes, and thus the plasma, extend further out around $x = 1.2$ mm, which is consistent with the x-ray image shown in Fig. 2. The inference of n_e from these measurements is discussed in the next section.

IV. ANALYSIS AND DISCUSSION

The spatial variation of the electron temperature along the line focus as inferred from Thomson scattering spectra and x-ray line ratios is presented in Fig. 6. The Thomson scattering results are space and time resolved; the temperatures shown correspond to $t = t_{peak} \pm 100$ ps and $z = 50$ μm, conditions similar to those for which x-ray laser gain is expected [27,28]. The uncertainty on the position at which the plasma is probed comes mainly from the focal spot diameter of the probe, which is 50 μm, and from the accuracy of the target position relative to the scattering volume, which is ± 25 μm. The location of that cell is also affected by the refraction of the probe beam. It is difficult to evaluate what the effect of refraction will be since it depends on the exact shape of the electron density profile. However, for the plasmas studied in this experiment, we estimate that for $n_e \leq 1 \times 10^{21}$

cm^{-3}, the deviation of the probe beam towards the lower densities does not exceed 30 μm. The density, at $z=50$ μm, estimated from interferometric measurements in spot-focus geometry and hydrodynamic simulations, is $\sim 5\times 10^{20}$ cm^{-3}.

The overall error bars of $\pm 15\%$ on the T_e values are due principally to the uncertainties connected with the fitting process. One of the problems encountered during this procedure was that the experimental spectra were often characterized by peaks broader than those of the calculated spectra. This then allows a certain range of values of T_e to fit the experimental data. We believe that the discrepancy between the width of the ion peaks in the calculated and experimental spectra is due in part to the fact that the only mechanism for the damping of the ion acoustic waves included in the theory [21] is ion Landau damping. For this study, the average charge of the plasma was $\bar{Z}=22\pm 1$ and T_i would have needed to be very large, $T_i \sim 1.5$ keV, for the ion Landau damping to account for the observed broadening. Other mechanisms, such as collisions or turbulence, could be responsible for the shape of the peaks in the experimental spectra.

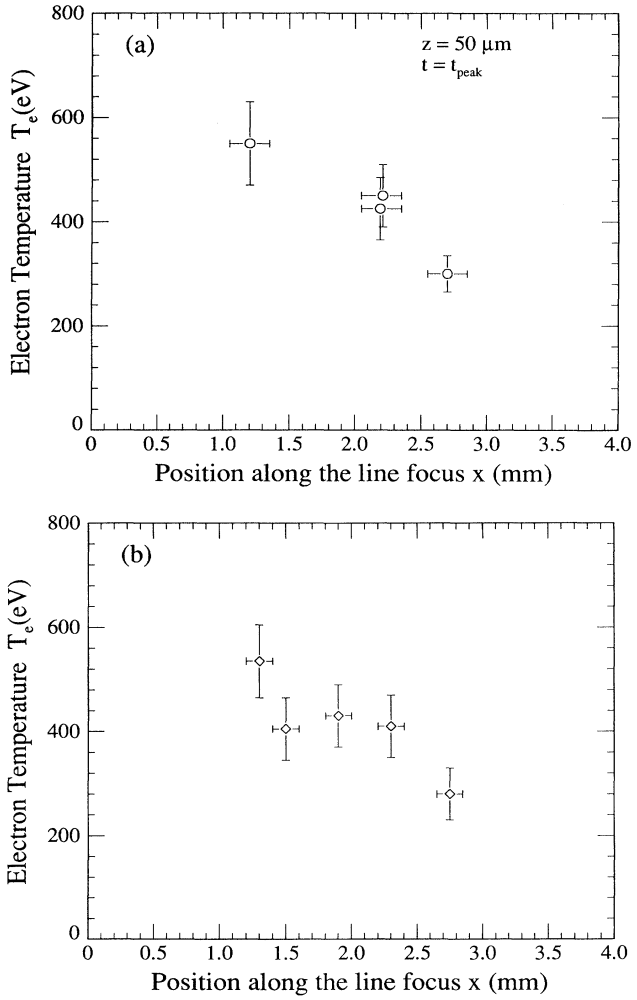

FIG. 6. (a) Variation of T_e along the line focus as inferred from space- and time-resolved Thomson scattering measurements. ($t=t_{peak}\pm 100$ ps and $z=50\pm 25$ μm). (b) Variation of T_e along the line focus as inferred from x-ray intensity ratios.

The temperatures obtained from the x-ray spectra are time integrated and spatially resolved in the direction of the x-ray laser axis. Although the emission is spatially integrated along the plasma expanding away from the target surface, it is expected to be strongly weighted towards the hot, dense region close to the critical surface. The maximum x-ray emission, as measured by the pinhole camera, occurs at $z=50\pm 10$ μm in front of the target plane where we measure T_e with the Thomson scattering diagnostic. Furthermore, the production and excitation of F-like Ge excited states will be maximized at the peak of the Gaussian pulse for the electron-temperature conditions studied here. Therefore a comparison of the x-ray spectroscopic T_e data with the time- and space-resolved Thomson scattering results is appropriate.

A local thermodynamic equilibrium (LTE) approximation [29] is applied to the higher quantum levels, in particular the $n=4\rightarrow 2$ Ne-like and F-like emission lines. The basic assumption here is that the collisional rates within these $n\geq 4$ levels are a factor of a few greater than the radiative rates. Various authors have used an LTE model with some success to describe the x-ray emission and measure electron temperature for a Ne-like Cu plasma [15] and a Ne-like Ge plasma [30]. We then use Boltzmann equations to deduce T_e from the intensity ratios of $4d\rightarrow 2p$ F-like resonance lines to $4d\rightarrow 2p$ and $4s\rightarrow 2p$ Ne-like resonance lines, labeled in Fig. 4. In order to use line ratios from different charge states, we have applied a detailed configuration accounting (DCA) model [31] to predict the charge-state distribution for Na-, Ne-, F-, and O-like germanium ions in steady state as a function of T_e at critical density, $n_e=10^{21}$ cm^{-3}. We have then assumed that the charge-state distribution at the measured T_e position of $z=50$ μm is largely determined by the ionization conditions at critical density; this is then "frozen" for the adjacent subcritical region. Typically, the temperature threshold for Ne-, F-, and O-like ion production is 150, 250, and 375 eV, respectively. The peak abundance is approximately 70% at 350 eV for Ne-like ions, 40% at 600 eV for F-like ions, and 30% at 770 eV for O-like ions. It should be noted that the temperature required to produce the various ion species will increase if there is significant ion production at densities lower than 5×10^{20} cm^{-3}.

We believe the strong Ne-like $4d\rightarrow 2p$ transitions at 7.081 and 7.203 Å in Fig. 4 are not suitable for line ratio comparisons on account of self-absorption and blending with Na-like satellites (for the line at 7.203 Å). We find 70% higher values for T_e from the Ne-like $4d\rightarrow 2p$ comparison. This is consistent with the interpretation of self-absorption on the strong 7.081-Å line. In fact, using an escape factor approximation [32], we estimate the optical depth to be large, $\tau>4$, for the $4d\rightarrow 2p$ transition and to be substantially less, $\tau<1$, for the $4s\rightarrow 2p$ transitions at 7.273 and 7.413 Å. Our main conclusion here is that self-absorption can strongly affect the atomic physics kinetics and observed emission of strong radiative transitions; plasma geometry here is very important. However,

careful choice of optically thin transitions can avoid these difficulties.

The errors for electron temperature shown in Fig. 6(b), derived from x-ray spectroscopy, come from a variety of sources. They are mainly from uncertainties in the film and other calibration factors. The use of the less intense F- and Ne-like transitions with radiative transition rates [33] of $\sim 10^{12}$ s^{-1}, although satisfying the LTE approximation, results in lower signal-to-noise ratios. Worst-case error bars of up to $\pm 25\%$ on the measured line ratios give an estimated $\pm 10\%$ uncertainty on T_e. An estimated error of $\pm 5\%$ on the oscillator strength ratios of selected lines makes a small contribution. The final error on T_e is about $\pm 20\%$.

Electron-temperature variations of approximately $\pm 40\%$ were observed to correlate with inhomogeneities in the intensity of the incident laser beam. Variations of $\pm 25\%$ in T_e were reported in a previous study of Cu plasmas in linear geometry with similar irradiance conditions [15]. The values obtained here are consistent with the variation of the ionization state observed along the line focus. Indeed, earlier work tends to indicate that there is a strong variation in the emission from F-like germanium ion transitions at laser intensities of 1 to 4×10^{13} W/cm^2 [26], for which electron temperatures comparable to those obtained in this experiment (~ 200–400 eV) have been measured [30]. Most previous results have related the x-ray emission to the local fluence on target [13,14,34,35], but no report of both electron-temperature and density measurements is available for collisional systems at this time, to the authors' knowledge.

The electron density can be estimated from the interferogram in Fig. 5. A density profile, along the line focus, at a distance $z = 160\pm 20$ μm in front of the target surface, at the peak of the pulse, is presented in Fig. 7. The density cannot be inferred at distances closer to the target surface because the fringes are blurred in that region. This blurring is caused principally by the rapid motion of the plasma and by refraction. The n_e values are obtained by simply counting the number of fringe shifts at different locations in the plasma and then assuming that the plasma was a uniform slab. The lateral dimension of that slab was taken to be 500 μm, in accordance with a measurement made in similar irradiance conditions, on a spot-focus plasma. In this way, a simple linear relation of the electron density to the measured fringe shift was obtained. The limitations of this procedure lie in the uncertainty of the lateral dimension of the plasma. Since there is a discrepancy between the interferometric measurements and the hydrocode simulations [36], the lateral extent of the plasma is known only within a factor of ~ 2. This results in a factor of 2 uncertainty on the absolute values of the electron density. However, the inferred relative variation of n_e along the x-ray laser axis will not be affected by this problem. The limiting assumption in this case is the uniformity of the lateral dimension of the plasma along the line. As a first-order approximation, we have assumed that this dimension was constant. The results then show a reasonably uniform spatial density distribution in the central part of the line focus. If one assumes that the plasma is wider where T_e is higher, the inferred electron density would be even more uniform along the line focus. Therefore, although the interferometry does not allow us to measure the density exactly at the place where we measure the temperature, it appears that the inhomogeneities of the density are not as significant as that of T_e.

The temporal evolution of the temperature is provided by the streaked Thomson scattering results. Figure 8 shows the time dependence of T_e for both line-focus ($x = 2.20\pm 0.15$ mm and $z = 50\pm 25$ μm) and spot-focus geometries ($z = 50\pm 25$ μm). From these results, it is clear that the geometry plays an important role in the decay of the temperature. For the line focus, it shows a

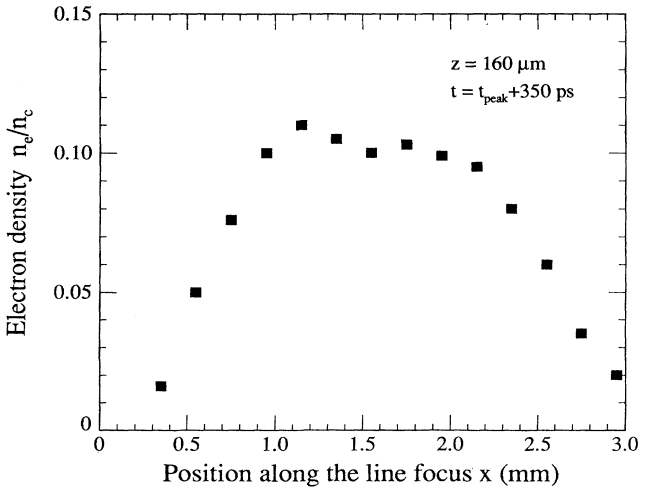

FIG. 7. Approximate electron density along the line focus, at a distance $z = 160\pm 20$ μm from the target surface and at $t = t_{peak} + 350\pm 200$ ps. In the figure, $n_c = 1\times 10^{21}$ cm^{-3} is the critical density for the pump laser.

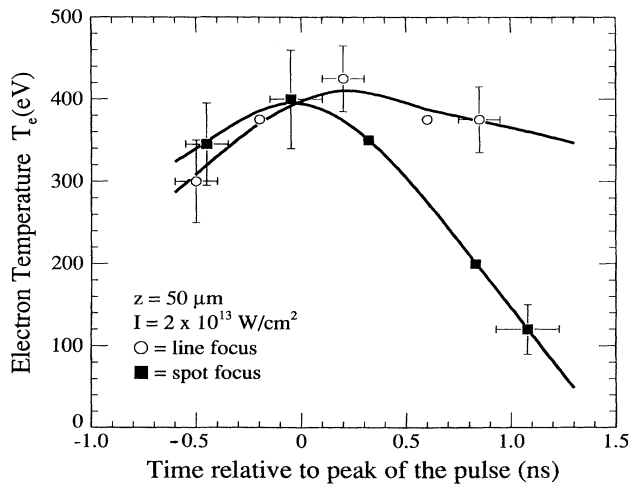

FIG. 8. Temporal evolution of the electron temperature in line- ($x = 2.20\pm 0.15$ mm and $z = 50\pm 25$ μm) and spot-focus geometry ($z = 50\pm 25$ μm). A slower decay of T_e after the peak of the laser pulse is observed for the line-focus plasma.

rapid increase of T_e up to the peak of the main laser pulse (t_{peak}), and than a slow decay $[1/T_{e,peak}(\partial T_e/\partial t) \simeq 0.15 \pm 0.05$ ns$^{-1}]$ in the following nanosecond. In the case of the spot focus, the decay is much faster $[1/T_{e,peak}\partial T_e/\partial t \simeq 0.65 \pm 0.10$ ns$^{-1}]$. This could be explained by the fact that in a spot focus the plasma can cool by expanding laterally in two dimensions, whereas for the line focus, the lateral expansion is important only on the axis perpendicular to the line focus. This could be significant for the duration of the gain in regions close to the ends of the line focus, where the cooling is expected to be faster. It also indicates that care must be taken in extrapolating spot-focus measurements to line-focus geometries.

Detailed modeling is needed to deduce how the x-ray gain varies with T_e and n_e because of the numerous plasma processes that can influence the ionic balance and the excited-state population distribution. If we use very simple assumptions, however, it is possible to get an idea of the relationship of the gain per unit length to T_e and n_e, for a narrow range of conditions.

We consider the $J=2 \rightarrow 1$ transition. By supposing that the pumping is due exclusively to collisional excitation, we can obtain an expression for the population inversion of the lasing transition which varies like $\exp(-\Delta E/kT_e)$, where ΔE is the excitation energy from the ground state to the upper lasing level. The neonlike ion population as calculated with a DCA code [37] also shows a weak dependence on T_e, for the irradiance conditions studied here. The gain coefficient will therefore be influenced mainly by T_e through the electron collision excitation rates. Thus the combined effects of the temperature and density inhomogeneities along the line focus can seriously degrade the gain. For instance, at the end of the line-focus plasma, the effects of a somewhat lower T_e and its faster decay combined with the electron density dropping considerably could severely reduce the gain in these regions. Also, for the zones inside the line focus where T_e drops by about 40% but where the density remains more or less constant, the gain coefficient can experience a reduction of $\sim 80\%$. These negative effects can probably be overcome by going to a saturation regime where the intensity and, thus, the temperature dependence becomes much less important [26]. However, to do that, one needs to use higher energies to pump the x-ray laser and, therefore, the efficiency is lowered considerably. Alternatively, the main laser intensity can be tailored along the line focus to achieve constant conditions. Another problem, which could arise due to the nonuniformity observed, is the refraction of the rays of the laser out of the gain region. This problem may become more serious for the $J=0 \rightarrow 1$ transition which is expected to have maximum gain at higher electron densities and earlier during the main laser pulse, when the gradients are steeper [26].

It should be noted that recent results obtained for gain on a core-excited transition were obtained with a special focusing arrangement that helped achieve a more uniform line focus [38]. For very similar irradiance conditions, this gain could more easily be observed in the plasma that was more homogeneous [9]. This may point to a possible scaling of the Ne-like systems towards the water window; for example, amplification of high-energy ($2p \rightarrow 2s$) transitions at 60–80 Å for germanium [39] predicted to have smaller gain coefficients ~ 1 cm^{-1} would require a homogeneous line focus.

In conclusion, a quantitative characterization of the inhomogeneities in a Ne-like x-ray laser plasma has been achieved. Space- and time-resolved Thomson scattering measurements of T_e have been used simultaneously with x-ray spectroscopy. The electron-temperature values obtained from line intensity ratios are in good agreement with the Thomson scattering results. The electron density uniformity was also monitored with interferometry. This study has revealed that the laser illumination nonuniformity affects the electron temperature more than the electron density. As a consequence, the inhomogeneity in T_e can degrade the overall gain or, at best, reduce the efficiency. The plasma uniformity is therefore a very important issue for the achievement of a true tabletop x-ray laser.

ACKNOWLEDGMENTS

The authors would like to acknowledge useful discussions with several people: S. Maxon, A. Osterheld, M. Prasad, M. D. Rosen, R. Walling of the Lawrence Livermore National Laboratory, and J. P. Matte of INRS-Énergie. They would also like to thank Y. T. Lee for making the screened hydrogenic version of this DCA code [31] available to us.

*Also at INRS-Énergie, C.P. 1020, Varennes, Quebec, Canada J3X 1S2.

†Present address: Lawrence Livermore National Laboratory, P. O. Box 808, Livermore, CA 94550.

[1] D. L. Matthews *et al.*, Phys. Rev. Lett. **54**, 110 (1985).

[2] M. D. Rosen, P. L. Hagelstein, D. L. Matthews, E. M. Campbell, A. U. Hazi, B. L. Whitten, B. J. MacGowan, R. E. Turner, R. W. Lee, G. Charatis, Gar. E. Busch, C. L. Shepard, and P. D. Rockett, Phys. Rev. Lett. **54**, 106 (1985).

[3] S. Suckewer, C. H. Skinner, H. Milchberg, C. Keane, and D. Voorhees, Phys. Rev. Lett. **55**, 1753 (1985).

[4] T. N. Lee, E. A. McLean, and R. C. Elton, Phys. Rev. Lett. **59**, 1185 (1987).

[5] C. Chenais-Popovics, R. Corbett, C. J. Hooker, M. H. Key, G. P. Kiehn, C. L. S. Lewis, G. J. Pert, C. Regan, S. J. Rose, S. Sadaat, R. Smith, T. Tomie, and O. Willi, Phys. Rev. Lett. **59**, 2161 (1987).

[6] B. J. MacGowan *et al.*, J. Appl. Phys. **61**, 5243 (1987).

[7] Raymond C. Elton, *X-Ray Lasers* (Academic, San Diego, 1990).

[8] H. Azuma, Y. Kato, K. Yamakawa, T. Tachi, M. Nishio, H. Shiraga, S. Nakai, S. A. Ramsden, G. J. Pert, and S. J. Rose, Opt. Lett. **15**, 1011 (1990).

[9] G. D. Enright, D. M. Villeneuve, J. Dunn, H. A. Baldis, J. C. Kieffer, H. Pépin, M. Chaker, and P. Herman, J. Opt.

Soc. Am. B **8**, 2047 (1991).
[10] S. Wang *et al.*, J. Opt. Soc. Am. B **9**, 360 (1992).
[11] Christopher J. Keane, in *Ultrashort Wavelength Lasers,* Proc. SPIE 1551, edited by S. Suckewer (Society of Photo-optical Instrumentation Engineers, Bellingham, WA, 1992), p. 2.
[12] M. D. Rosen, Phys. Fluids B **2**, 1461 (1990).
[13] P. Jaeglé, P. Dhez, A. Klisnick, A. Carillon, G. Jamelot, B. Gauthé, J. P. Raucourt, P. Goedtkindt, and J. C. Kieffer, in *Optical Society of America Proceedings on Short-Wavelength Coherent Radiation,* edited by P. A. Bucksbaum and N. M. Ceglio (Optical Society of America, Washington, DC, 1991), Vol. 11, p. 123.
[14] J. C. Kieffer, M. Chaker, H. Pépin, M. Nantel, H. A. Baldis, J. Dunn, G. D. Enright, and D. M. Villeneuve, Opt. Commun. **84**, 208 (1991).
[15] R. C. Elton, T. N. Lee, and W. A. Molander, J. Opt. Soc. Am. B **4**, 539 (1987).
[16] J. Dunn, H. A. Baldis, G. D. Enright, B. La Fontaine, D. M. Villeneuve, J. C. Kieffer, H. Pépin, M. Nantel, and M. Chaker, in *Ultrashort Wavelength Lasers,* Ref. [11].
[17] B. L. Henke, J. Y. Uejio, G. F. Stone, C. H. Dittmore, and F. G. Fujiwara, J. Opt. Soc. Am. B **3**, 1540 (1986).
[18] R. Hall, Ph.D. thesis, University of Leicester, Leicester, England (1980).
[19] B. L. Henke, P. Lee, T. J. Tanaka, R. L. Shimabukuro, and B. K. Fujikawa, At. Data Nucl. Data Tables **27**, 1 (1982).
[20] B. L. Henke, S. L. Kwok, J. Y. Uejio, H. T. Yamada, and G. C. Young, J. Opt. Soc. Am. B **1**, 828 (1984).
[21] John Sheffield, *Plasma Scattering of Electromagnetic Radiation* (Academic, New York, 1975).
[22] D. E. Evans and J. Katzenstein, Rep. Prog. Phys. **32**, 207 (1969).
[23] H. A. Baldis, B. La Fontaine, J. Dunn, G. D. Enright, D. M. Villeneuve, M. D. Rosen, and D. L. Matthews, in *Ultrashort Wavelength Lasers,* Ref. [11], p. 114.
[24] B. La Fontaine, H. A. Baldis, D. M. Villeneuve, J. E. Bernard, G. D. Enright, P. E. Young, and D. L. Matthews, in *X-Ray Lasers,* Institute of Physics Conference Series 116, edited by G. J. Tallents (IOP Publishing, London, 1991), p. 9.
[25] J. E. Bernard, H. A. Baldis, D. M. Villeneuve, and Kent Estabrook, Phys. Fluids **30**, 3616 (1987).
[26] D. M. O'Neill, C. L. S. Lewis, D. Neely, J. Uhomoibhi, M. H. Key, A. MacPhee, G. J. Tallents, S. A. Ramsden, A. Rogoyski, E. A. McLean, and G. J. Pert, Opt. Commun. **75**, 406 (1990).
[27] D. Neely, C. L. S. Lewis, J. Uhomoibhi, D. M. O'Neill, S. A. Ramsden, M. H. Key, B. Shiwai, N. Tragin, and G. J. Tallents, Annual Report No. RAL-90-026, Central Laser Facility, Oxford University, 1990 (unpublished).
[28] D. Neely, C. L. S. Lewis, D. M. O'Neill, J. Uhomoibhi, S. A. Ramsden, G. J. Tallents, Y. A. Hadithi, M. H. Key, S. J. Rose, and G. J. Pert, Annual Report No. RAL-91-025, Central Laser Facility, Oxford University, 1991 (unpublished).
[29] Hans R. Griem, *Plasma Spectroscopy* (McGraw-Hill, New York, 1964).
[30] Guo-bin Ma, Yuan Gu, Shi-ji Wang, Guo-qiang Han, Xin Wang, Yun-feng Shao, and Yang-hui Qiu, Phys. Rev. A **43**, 1972 (1991).
[31] Y. T. Lee, J. Quant. Spectrosc. Radiat. Transfer **38**, 131 (1987).
[32] F. P. Keenan and A. E. Kingston, Mon. Not. R. Astron. Soc. **220**, 493 (1986).
[33] Radiative transition rates for Ne-like and F-like ion $n=3,4,5$ levels were calculated by Rosemary Walling (private communication).
[34] J. C. Kieffer, M. Chaker, H. Pépin, H. A. Baldis, G. D. Enright, B. La Fontaine, and D. M. Villeneuve, Phys. Fluids B **3**, 463 (1991).
[35] Zhi-zhan Xu, P. H. Y. Lee, Li-huang Lin, Wei-qing Zhang, Zhi-ming Jiang, Shao-xian Meng, Jia-jin Yu, and Ai-di Qian, Opt. Commun. **61**, 199 (1987).
[36] M. D. Rosen, S. Maxon, and M. Prasad (private communication).
[37] Jean-Pierre Matte (private communication).
[38] D. M. Villeneuve, G. D. Enright, H. A. Baldis, and J. C. Kieffer, Opt. Commun. **81**, 54 (1991).
[39] G. D. Enright, H. A. Baldis, J. Dunn, B. La Fontaine, D. M. Villeneuve, J. C. Kieffer, H. Pépin, and M. Chaker, in *Short-Wavelength Coherent Radiation,* Ref. [13], Vol. 11, p. 87.

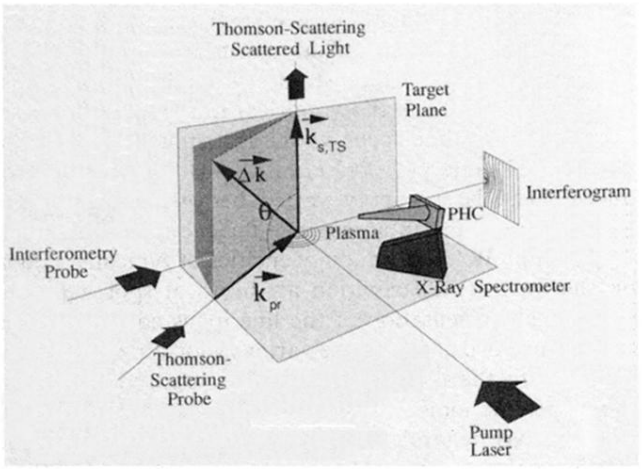

FIG. 1. Experimental setup. The diagnostics used were Thomson scattering of a uv probe by the plasma, x-ray spectroscopy, interferometry, and x-ray imaging. The vector diagram for Thomson scattering is shown. The line focus could be oriented either horizontally or vertically.

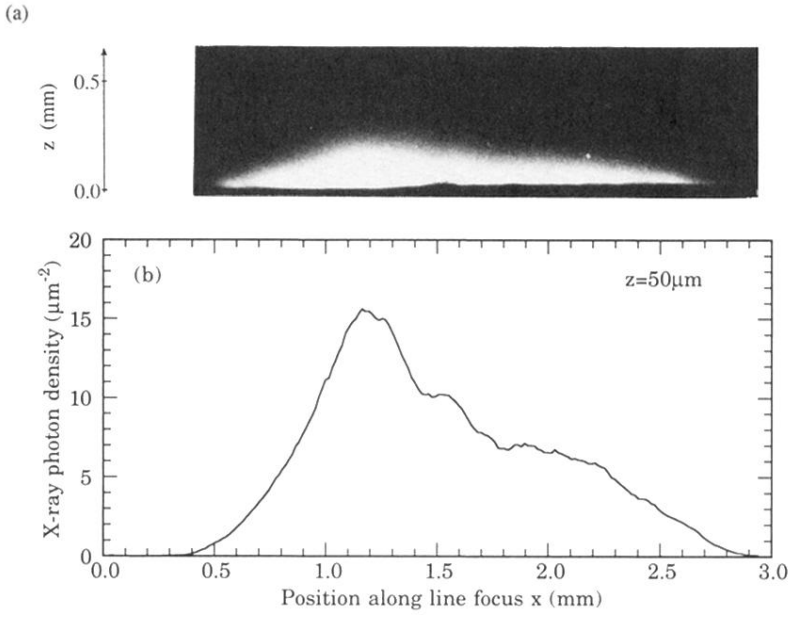

FIG. 2. This line rendition of the x-ray image of the line-focus plasma taken at $z = 50 \pm 10$ μm from the target plane shows the inhomogeneities along the line focus. The x-ray photon density is expressed in photons/μm^2 at the film plane.

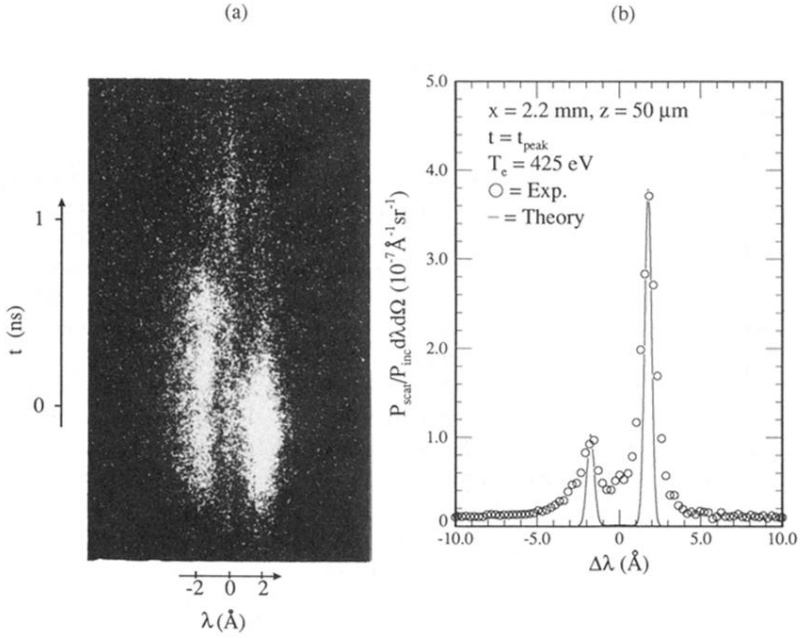

FIG. 3. Thomson scattering spectrum from Ne-like Ge x-ray laser plasma. $I = 1 \times 10^{13}$ W/cm^2, $x = 2.20 \pm 0.15$ mm, and $z = 50 \pm 25$ μm. (a) Streak record showing the two peaks of the ion feature. (b) Intensity profile taken at $t = 0 \equiv t_{peak}$. ($T_e = 425 \pm 60$ eV.)